Endocrine Journal 2011, **58** (3), 193-198

ORIGINAL

Hypopituitarism in a patient with transsphenoidal cephalocele: longitudinal changes in endocrinological abnormalities

Keiji Tanimoto, Saori Onda, Hideaki Sawaki, Tetsuya Hiraiwa, Hiroyuki Sano, Mineki Ohnishi, Jungo Terasaki and Toshiaki Hanafusa

Department of Internal Medicine (I), Osaka Medical College, Takatsuki 569-8686, Japan

Abstract. We report a 21-year-old man with severe fatigue due to hypopituitarism. At the age of 6 years, he was diagnosed with short stature due to a GH deficiency accompanied by a sphenoid cystic lesion. Laboratory findings and provocative tests for pituitary hormone function revealed ACTH, LH, FSH, TSH, and GH deficiency. Computed tomography and magnetic resonance imaging revealed transsphenoidal cephalocele due to a defect in the floor of the sella turcica. At 6 years, he only had severe GH deficiency and poor response of LH to LHRH. Hypothalamic-pituitary dysfunction and pituitary herniation have progressed subsequently; we observed a longitudinal progression of hypothalamic-pituitary dysfunction caused by transsphenoidal cephalocele. This dysfunction requires the selection of a treatment that will not aggravate the condition further.

Key words: Hypothalamic-pituitary dysfunction, Panhypopituitarysm, Pituitary herniation, Follow-up, MRI

CONGENITAL basal encephaloceles are rare, with an estimated incidence of 1 in every 35,000 live births [1]. Transsphenoidal cephalocele is the least frequent anomaly, representing only 5% of basal encephaloceles (estimated incidence: 1 in 700,000 live births). In transsphenoidal cephalocele, transsphenoidal lesions collapse into the epipharynx or nasopharynx [2]. The diagnosis of transsphenoidal cephalocele is usually made in infancy or early childhood [3].

Because the floor of the sella turcica is lacking in this anomaly, hypothalamic-pituitary function may deteriorate. The natural course of hypothalamic-pituitary dysfunction due to transsphenoidal cephalocele remains unclear. There are only a few reports describing endocrinological follow-up due of transsphenoidal cephalocele for a period of 10 years or more. We report the longitudinal progression of hypothalamic-pituitary dysfunction due to transsphenoidal cephalocele in a patient. Surgical treatment for transsphenoidal cephalocele was not performed in the follow-up period; the natural course of hypothalamic-pituitary dysfunction was able to be observed.

Received Dec. 24, 2010; Accepted Jan. 19, 2011 as K10E-405
Released online in J-STAGE as advance publication Feb. 17, 2011

Correspondence to: Keiji Tanimoto, Department of Internal Medicine (I), Osaka Medical College, 2-7 Daigaku-machi, Takatsuki city, Osaka 569-8686, Japan
E-mail: in1120@poh.osaka-med.ac.jp

Case Report

A 21-year-old man was referred to our hospital with severe fatigue. At 6 years of age, he had consulted the department of pediatrics in our hospital because of his short height (97.4 cm, −3.56 SD). He was diagnosed with short stature due to GH deficiency accompanied by a sphenoid cystic lesion. Until 10 years old, he did not visit his doctor. GH replacement therapy was administered from the age of 10 to 13 years. However, the patient could not continue the GH replacement therapy after the age of 13 years. After this, he visited the doctor about only once a year, and he did not receive a treatment. At 21 years of age, he was hospitalized in a local hospital due to infectious enteritis; he was also diagnosed with secondary hypothyroidism. Following this, he was admitted to our hospital for further evaluation of hypopituitarism.

His height was 144 cm and body weight was 38 kg. He had no external malformations, but had peripapillary staphyloma in left eye. No axillary or pubic hair was present. His Tanner stages were G1 and P1, and each of his testes was 3 mL in volume. The labora-

Table 1 Laboratory findings

White blood cell	5620 /μL
Neutrophil	62.9 %
Lymphocyte	28.6 %
Eosinophil	3.2 %
Red blood cell	359 × 10^4 /μL
Hemoglobin	10.2 g/dL
Hematocrit	30.3 %
Platelet	25.4 × 10^4 /μL
Albumin	4.2 g/dL
Aspartate aminotransferase	24 IU/L
Alanine aminotransferase	13 IU/L
Lactate dehydrogenase	204 IU/L
Creatinine kinase	83 IU/L
Alkaline phosphatase	254 IU/L
Blood urea nitrogen	6 mg/dL
Creatinine	0.56 mg/dL
Uric acid	4.2 mg/dL
Total-Cholesterol	200 mg/dL
Triglyceride	105 mg/dL
Sodium	141 mEq/L
Potassium	3.9 mEq/L
Chloride	108 mEq/L
Calcium	8.9 mg/dL
Fasting serum glucose	84 mg/dL

Table 2 Endocrinological laboratory findings

		Reference value
TSH	2.790 μU/mL	(0.500~5.000)
Free T3	1.62 pg/mL	(2.30~4.30)
Free T4	0.77 ng/dL	(0.90~1.70)
PRL	11.26 ng/mL	(3.58~12.78)
GH	0.08 ng/mL	(<0.17)
IGF-I	12 ng/mL	(133~368)
ACTH	13.0 pg/mL	(7.2~63.3)
Cortisol	4.7 μg/dL	(4.0~18.3)
DHEA-S	8 μg/dL	(85~690)
UFC	8.1 μg/day	(11.2~80.3)
LH	<0.1 mIU/mL	(0.79~5.72)
FSH	0.3 mIU/mL	(2.00~8.30)
Testosterone	<0.05 ng/mL	(2.07~7.61)
Plasma Osm	279 mOsm/kg	(276~292)
Urine Osm	350 mOsm/kg	(50~1200)
ADH	1.0 pg/mL	(0.3~3.5)

Free T3: free triiodothyronine, Free T4: free thyroxine, IGF-I: insulin-like growth factor-I, ADH: antidiuretic hormone, DHEA-S: dehydroepiandrosterone sulfate, UFC: urinary free cortisol

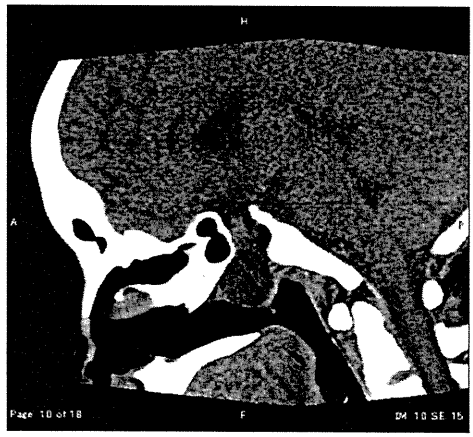

Fig. 1 Sagittal head CT demonstrated a bone defect in the floor of the sella turcica by a transsphenoidal soft tissue mass extending into the epipharynx.

tory examination is displayed in Table 1. Red blood cell, hemoglobin, and hematocrit decreased slightly. Endocrinological laboratory findings are shown in Table 2. Although the serum levels of both free triiodothyronine and free thyroxine were low, TSH was normal. IGF-I (insulin-like growth factor-I) level was low for his age and sex; IGF-I SD score was −5.7 SD. Levels of plasma ACTH, serum cortisol and dehydroepiandrosterone sulfate (DHEA-S), and urinary free cortisol were all low. LH and testosterone levels were lower than the measurable limit. Provocative tests for pituitary hormone function are shown in Table 3. The response of cortisol to 250 μg of synthetic ACTH was impaired; the peak value of cortisol was 12.9 μg/dL. Both LH and FSH levels were consistently low in response to LHRH injection. After TRH administration, TSH rose to high values, but total T3 levels did not rise enough to 1.3 times or more. These findings suggested that bioactivity of TSH is decreased in the patient. The patient had almost no response of GH after GHRP-2 (growth hormone releasing peptide-2) injection. According to hand X-rays, his bone age was equivalent to a 12.6-year-old Japanese boy. Computed tomography (CT) of the head showed a defect in the floor of the sella turcica (Fig. 1.). Magnetic resonance imaging (MRI) revealed a cystic mass extending into the epipharynx through the bone defect (Fig. 2a and 2b).

On the basis of the above mentioned findings, he was diagnosed with ACTH, LH, FSH, TSH, and GH

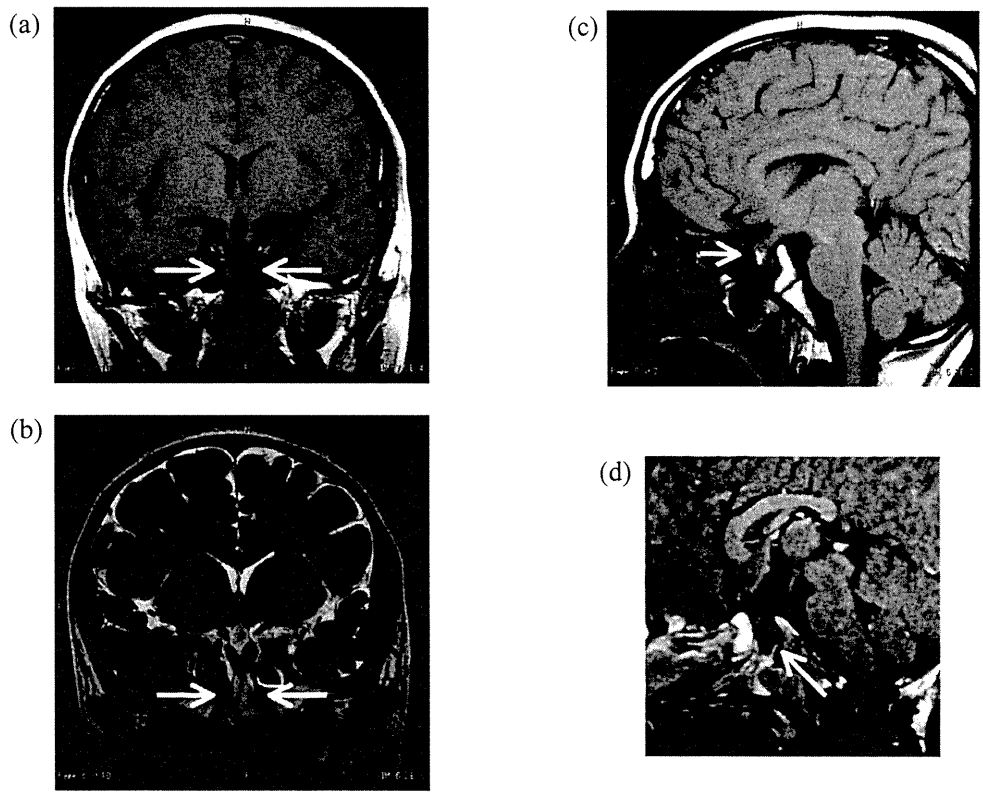

Fig. 2 T1-weighted (a) and T2-weighted (b) coronal and T1-weighted sagittal (c) MRI revealed a cystic mass with a surrounding structure extending through the bone defect into the epipharynx. The longitudinal diameter of the cystic mass was 3.5 centimeters. T1-weighted sagittal MRI at the age of 6 years (d) demonstrated a sphenoid cystic lesion 1.5 centimeters in diameter.

deficiency due to transsphenoidal cephalocele. Nasal obstruction or nasal discharge, meningitis, and cerebrospinal fluid rhinorrhea were not present; therefore, he did not undergo surgery. He received replacement therapy of adrenocortical hormone (hydrocortisone 20 mg), thyroid hormone (levothyroxine sodium hydrate 75 μg), after which his complaints were resolved. His weight was increased to 44kg, though his height did not change. Ten months after, he accepted the replacement therapy of sex hormone (testosterone enanthate 125mg, once a month) and GH (somatropin 1.3mg). However, he did not come to our hospital three months later.

Discussion

Transsphenoidal cephalocele often leads to hypothalamic-pituitary dysfunction. The incidence of hypothalamic-pituitary insufficiency was estimated at about 50–60% in previous reports [1, 4, 5]. Hypothyroidism, GH deficiency, hypogonadotrophic hypogonadism, and diabetes insipidus were frequent disorders. Central hypoadrenalism was rare in previous reports [6]. In our case, hypothyroidism, GH deficiency, hypogonadotrophic hypogonadism, and hypoadrenalism were found, but diabetes insipidus was not detected from laboratory findings and MRI (Table 2 and Fig. 2c).

We obtained the clinical examination data from the hospital where this patient had consulted a doctor in his childhood. Results of his endocrinological examination at the age of 6 years are shown in Table 4. Severe GH deficiency and poor response of LH to LHRH were observed. No evidence of ACTH, FSH, TSH, or ADH deficiency was present at that point. He was diagnosed with short stature due to GH deficiency. His subsequent clinical course is shown in Fig. 3. Free T4 level decreased gradually; nevertheless, TSH did not rise sufficiently. Testosterone levels were lower than the measurable limit at all time points. By the time he was admitted to our hospital at the age of 21, he

Table 3 Provocative tests for pituitary hormone function

	Before	15 min	30 min	45 min	60 min	90 min	120 min
ACTH (250 μg) administration test							
Cortisol (μg/dL)	2.8		11.6		12.9		
CRH (100 μg), LHRH (100 μg), and TRH (200 μg) administration test							
ACTH (pg/mL)	40.2		124		88.1	86.8	
Cortisol (μg/dL)	10.3		17.5		17.8	21.3	
LH (mIU/mL)	0.2		0.4		0.4	0.4	
FSH (mIU/mL)	0.7		1.2		1.4	1.6	
TSH (μU/mL)	8.65		27.7		25.7	21.2	
PRL (ng/mL)	20.7		28.3		22.0	17.7	
Total T3 (ng/mL)	0.75						0.97
GHRP-2 (growth hormone releasing peptide-2) (100 μg) administration test							
GH (ng/mL)	<0.03	0.12	0.08	0.04			

Table 4 Endocrinological findings when the patient was 6 years old

IGF-I	38 ng/mL	Total T4	12.9 μg/dL	Plasma Osm	279 mOsm/kg
Overnight GH	3.85 ng/mL (Mean)	Testosterone	<0.05 ng/mL	Urine Osm	799 mOsm/kg
				ADH	2.0 pg/mL

	Before	15 min	30 min	60 min	90 min	120min	150min
Insulin tolerance test (1.8U, 0.1U/kg)							
Glucose (mg/dL)	82	22	50	80	92		
GH (ng/mL)	0.41		1.4	1.2	0.3		
Cortisol (μg/dL)	11.4			26.0			
Propranolol-Glucagon administration test							
Glucose (mg/dL)	84		122	92	81	66	70
GH (ng/mL)	0.66		0.74	0.64	1.2	2.8	3.4
CRH (27 μg), LHRH (36 μg), and TRH (180 μg) administration test							
Cortisol (μg/dL)	12.6			21.5			
LH (mIU/mL)	<0.5		1.8	1.3	1.4		
FSH (mIU/mL)	0.8		4.0	4.2	5.9		
TSH (μU/mL)	2.7		13.0	8.7			
PRL (ng/mL)	4.3		13.0	7.6			

had not only GH deficiency, but also ACTH, LH, FSH, and TSH deficiency. MRI when he was 6 years old revealed a sphenoid cystic lesion 1.5 cm in diameter (Fig. 2d). The size of his transsphenoidal cephalocele had increased to 3.5 cm by the time of his admission to our hospital (Fig. 2a, 2b, and 2c). To summarize, both hypothalamic-pituitary dysfunction and pituitary herniation had progressed significantly in 15 years.

There are only a few case reports showing endocrinological follow-up for a time period of ten years or more in patients with transsphenoidal cephaloceles and pituitary herniation [2, 4, 7]. The natural course of hypothalamic-pituitary dysfunction is still unclear. Although hypothalamic-pituitary function was not necessarily examined at the first visit or during the follow-up time in all previous case reports, it has been reported that most patients (7 out of 9 patients: 77.8%) with transsphenoidal cephaloceles exhibited a progression of hormonal disturbances [8]. On the other hand, neurosurgical intervention could not effectively prevent pituitary dysfunction [4, 9]. In hypothalamic-pituitary dysfunction, surgical treatment might be required to prevent a progression of hormonal insufficiency. Since a valid surgical procedure for transsphe-

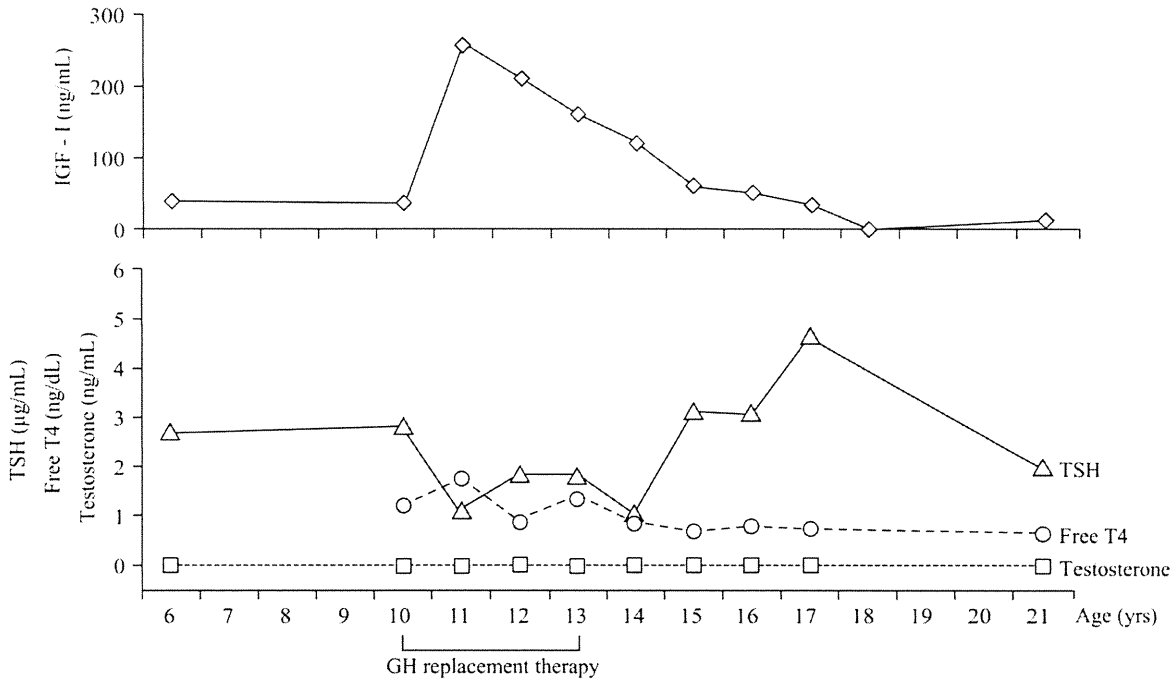

Fig. 3 Clinical course of endocrinological abnormality from 6 years to 21 years is shown. IGF-I (◇) rose temporarily in response to the GH replacement therapy. Free T4 (○) decreased gradually; nevertheless, TSH (△) did not rise appropriately. Testosterone (□) levels were lower than the measurable limit at all time points.

noidal encephalocele was recently reported, the number of treatable cases will probably increase in the near future [10-12].

The surgical treatment for transsphenoidal encephalocele has not always been beneficial [3, 13]. There is a risk of damaging the functioning tissue within the wall of encephalocele [10]. In our case, MRI revealed that a cystic mass contained a surrounding structure, and the pituitary hormones were not completely lack. In addition, surgical treatment could not effectively prevent pituitary dysfunction [4, 9]. If there was an evidence of respiratory obstruction, meningitis, cerebrospinal fluid rhinorrhea, and progressive visual defects, we will conduct a surgical repair to transsphenoidal encephalocele.

The mechanism of this hormonal abnormality is still unknown. In a child with diabetes insipidus complicated by cephalocele, the degeneration of the hypothalamus and agenesis of the supraoptic nuclei may be detected, but the description of pituitary gland anomaly had not been reported [2]. One report described a male patient with GH, TSH, and LH deficiency, and pituitary fibrosis, but a normal hypothalamus [4]. Therefore, the abnormalities of the hypothalamus and pituitary gland are variable. In the present case, MRI revealed that the periphery of the cephalocele was enhanced by gadolinium, and the posterior pituitary bright spot was observed in the sella turcica (Fig. 2). These findings suggest that both the anterior pituitary gland and the neurohypophysis existed. Accordingly, damage to the pituitary stalk might have caused hypothalamic-pituitary dysfunction in this case.

In conclusion, we have reported a patient who had ACTH, LH, FSH, TSH, and GH deficiency due to a transsphenoidal cephalocele. Both hypothalamic-pituitary dysfunction and pituitary herniation have gradually progressed in the past 15 years. In the future, surgical treatment might be a promising choice to prevent further progression of hormonal insufficiency in similar patients.

Acknowledgments

We would like to thank Dr. Kazutaka Konishi, Abuyama Pediatrics Clinic, and Dr. Okasora Keisuke, Department of Pediatrics, Hirakata Municipal Hospital, for providing the childhood clinical data of this patient.

References

1. Smith DE, Murphy MJ, Hitchon PW, Babin RW, Abu-Yousef MM (1983) Transsphenoidal encephaloceles. *Surg Neurol* 20: 471-480.
2. Pollock JA, Newton TH, Hoyt WF (1968) Transsphenoidal and transethmoidal encephaloceles. A review of clinical and roentgen features in 8 cases. *Radiology* 90: 442-453.
3. Yokota A, Matsukado Y, Fuwa I, Moroki K, Nagahiro S (1986) Anterior basal encephalocele of the neonatal and infantile period. *Neurosurgery* 19: 468-478.
4. Ellyin FM, Potchynok A, Song C (1991) Long-term follow-up of hypothalamic-pituitary function in patients with transsphenoidal pituitary herniation and midfacial anomalies. *Clin Endocrinol (Oxf)* 35: 263-266.
5. Koral K, Geffner ME, Curran JG (2000) Transsphenoidal and sphenoethmoidal encephalocele: report of two cases and review of the literature. *Australas Radiol* 44: 220-224.
6. Lieblich JM, Rosen SE, Guyda H, Reardan J, Schaaf M (1978) The syndrome of basal encephalocele and hypothalamic-pituitary dysfunction. *Ann Intern Med* 89: 910-916.
7. Durham LH, Mackenzie IJ, Miles JB (1988) Transphenoidal meningohydroencephalocoele. *Br J Neurosurg* 2: 407-409.
8. Morioka M, Marubayashi T, Masumitsu T, Miura M, Ushio Y (1995) Basal encephaloceles with morning glory syndrome, and progressive hormonal and visual disturbances: case report and review of the literature. *Brain Dev* 17: 196-201.
9. Sailer HF, Landolt AM (1987) A new method for the correction of hypertelorism with preservation of the olfactory nerve filaments. *J Craniomaxillofac Surg* 15: 122-124.
10. Tsutsumi K, Asano T, Shigeno T, Matsui T, Ito S, Kaizu H (1999) Transcranial approach for transsphenoidal encephalocele: report of two cases. *Surg Neurol* 51: 252-257.
11. Abe T, Ludecke DK, Wada A, Matsumoto K (2000) Transsphenoidal cephaloceles in adults. A report of two cases and review of the literature. *Acta Neurochir (Wien)* 142: 397-400.
12. Faggin R, Pentimalli L, Grazzini M, Saetti R, Drigo P, d'Avella D (2009) Combined endoscopic-microsurgical approach for transsphenoidal (sphenopalatine) encephalocele with an intralesional pituitary gland. Case report. *J Neurosurg Pediatr* 4: 262-265.
13. David DJ (1993) Cephaloceles: classification, pathology, and management--a review. *J Craniofac Surg* 4: 192-202.

Mod Rheumatol (2011) 21:32–36
DOI 10.1007/s10165-010-0342-2

ORIGINAL ARTICLE

Therapeutic drug monitoring of cyclosporine microemulsion in interstitial pneumonia with dermatomyositis

Koji Nagai · Tohru Takeuchi · Takuya Kotani · Kenichiro Hata · Shuzo Yoshida · Kentaro Isoda · Youhei Fujiki · Hideyuki Shiba · Shigeki Makino · Toshiaki Hanafusa

Received: 27 January 2010 / Accepted: 6 July 2010 / Published online: 4 August 2010

Abstract The prognosis of dermatomyositis (DM)-associated progressive interstitial pneumonia (IP) has recently been improved by steroids/cyclosporine-A (CSA) combination therapy, but treatment outcomes varied. One reason for this variation is thought to be differences in CSA regimen. There is marked interpatient variability in CSA absorption. However, the pharmacokinetics of CSA has rarely been studied. In this study, we calculated the area under the blood concentration–time curve (AUC) of CSA microemulsion in 15 patients with progressive IP complicating DM, and analyzed its correlation with CSA levels at blood sampling time points to investigate the optimum monitoring and dosing regimen. The highest correlation between AUC_{0-6} and blood level of CSA was observed 2 h (C2) after drug administration ($R = 0.910$). The trough level (C0) was not correlated with AUC_{0-6} ($R = 0.052$). There were no differences in blood levels (AUC_{0-6}, C2, and C6) between postprandial administration in a divided dose (CSA given twice daily) and preprandial administration once daily in a single dose, while C0 was significantly lower ($P = 0.020$) when the drug was administered once daily before breakfast. These findings suggest that measurement of CSA blood level, especially C2 and C0, is useful to monitor clinical and adverse effects of CSA during combination therapy. It is also suggested that preprandial, once daily administration of CSA is beneficial in DM patients with progressive IP.

K. Nagai · T. Takeuchi (✉) · T. Kotani · K. Hata · S. Yoshida · K. Isoda · Y. Fujiki · H. Shiba · S. Makino · T. Hanafusa
First Department of Internal Medicine, Osaka Medical College, 2-7 Daigaku-Machi, Takatsuki, Osaka 569-8686, Japan
e-mail: t-takeuchi@poh.osaka-med.ac.jp

Keywords Cyclosporine · Dermatomyositis · Interstitial pneumonia · Monitoring

Introduction

Dermatomyositis (DM) is an idiopathic inflammatory muscular disease characterized by heliotrope-like erythema and Gottron's sign. Interstitial pneumonia (IP) often complicates DM (DM-IP) and progresses acutely/subacutely. It is resistant to steroids, and prognosis is poor [1]. Recent reports have revealed that a combination therapy of steroids and cyclosporine-A (CSA) was effective for progressive DM-IP, but the survival rate (42–69%) and efficacy varied [2–4]. One reason for this variation is thought to be differences in timing of administration and the dose of CSA.

CSA binds to calcineurin with cyclophilin and inhibits T-cell signals, exhibiting an immunosuppressive effect. Absorption of CSA varied widely between individuals, and therefore its blood level is frequently monitored. In the field of transplantation, the area under the blood concentration–time curve (AUC_{0-4} and AUC_{0-6}) of CSA have been highly correlated with adverse and clinical effects [5, 6]. However, frequent measurement of blood CSA level is necessary to calculate AUC, which is unsuitable for ordinary medical examination. In the transplantation field, the trough level (C0) is measured to prevent adverse drug reactions, and the level at 2 h after administration (C2) has recently been used to achieve immunological effect because of its correlation with AUC [7]. However, no study on pharmacokinetics of CSA has been reported in the field of collagen vascular disease (CVD).

In this study, we initially measured the CSA blood level after oral CSA administration in patients with progressive

DM-IP, calculated AUC_{0-6}, and identified the optimum blood sampling time point. We also investigated the influence of dosing regimen on the CSA blood level.

Patients and methods

Patients

Of 29 patients who underwent CSA administration for progressive DM-IP between December 1995 and December 2008, the study was performed in 15 patients in whom AUC_{0-6} could be measured. All 15 patients gave informed consent to this pharmacological study. Oral CSA was administered until December 2005 to 10 patients twice daily, after breakfast and dinner (the divided dose), at a rate of 4.0 mg/kg/day, concomitantly with 1 mg/kg/day prednisolone. From January 2006, 4.0 mg/kg/day CSA was administered once daily (before breakfast) concomitantly with 1 mg/kg/day prednisolone in 5 patients (single dose).

Measurement of blood concentrations of CSA and calculation of AUC

Blood samples for AUC determination were collected before administration (C0), and at 2-h intervals for 6 h after CSA administration (C2, C4, and C6, respectively). Blood CSA concentrations were measured by CSA monoclonal whole-blood assay (Cyclosporine-SP-Dynapack, Abbott Laboratories, Chicago, IL, USA) using a fluorescence polarization immunoassay kit. AUC_{0-6} (ng h/ml) was calculated by the trapezoidal method according to the formula $AUC_{0-6} = C0 + 2(C2 + C4) + C6$.

Statistical analysis

Correlations between AUC_{0-6} and C0, C2, C4, and C6 were assessed using the Pearson correlation coefficient. Simple comparisons of the means and standard error (SE) of data were performed using Student's t test. A P value <0.05 was considered significant. Statistical calculations were performed using JMP version 8.0.

Results

Patient profiles

Clinical findings, laboratory findings, and CSA treatment of DM patients with progressive IP are listed in Table 1. Their mean age was 55.3 years (range 43–68 years). Poor prognostic factors of DM with progressive IP include clinically amyopathic DM (C-ADM), creatine kinase (CK)/lactate dehydrogenase (LDH) ratio <2, negative test results with anti-Jo-1 antibodies, and presence of pneumomediastinum [2, 8]. Ten patients had C-ADM and CK/LDH ratio <2, 10 patients had negative test results with anti-Jo-1 antibodies, and pneumomediastinum was a complication in 3 of the 15 patients. One patient with postprandial administration of CSA died of IP progression. The mean KL-6 was 1250.9

Table 1 Patient profiles

Case	Age (years)	Sex	Diagnosis	Hugh–Jones classification	Complications	Cr (mg/dl)	CK/LDH ratio	Anti-Jo-1 antibody	KL-6 (U/ml)	Drug administration	Cy-A dosage (mg/day)	Outcome
1	61	M	P	V	Gastric cancer	0.92	191/659	–	3880	Post	200	Alive
2	52	M	P	III	–	0.93	265/344	–	2770	Post	250	Alive
3	47	M	P	IV	Pneumomediastinum	0.67	224/876	–	1220	Post	225	Alive
4	68	F	P	III	–	0.56	194/425	–	512	Post	175	Dead
5	43	F	D	III	–	0.43	9100/960	+	740	Post	175	Alive
6	50	F	D	IV	–	0.58	320/451	–	1630	Post	175	Alive
7	56	F	D	III	–	0.44	13574/1463	+	337	Post	200	Alive
8	61	F	P	V	–	0.5	490/726	–	739	Post	200	Alive
9	58	F	D	II	Acute respiratory distress syndrome	0.5	1820/811	–	712	Post	175	Alive
10	60	F	P	IV	–	0.58	1549/648	+	366	Post	225	Alive
11	54	F	D	IV	–	0.42	3075/655	+	997	Pre	175	Alive
12	52	F	P	IV	Pneumomediastinum	0.43	50/396	–	978	Pre	250	Alive
13	54	M	P	II	Pneumomediastinum	0.68	530/381	+	1900	Pre	225	Alive
14	56	F	D	III	–	0.4	257/269	–	713	Pre	275	Alive
15	58	F	P	IV	–	0.45	553/438	–	1270	Pre	200	Alive
Average	55.3					0.57			1250.9		208.3	

P probable DM; *D* definite DM; *Cr* creatinine; *CK* creatine kinase; *LDH* lactate dehydrogenase; *Post* postprandial, twice daily in a divided dose; *Pre* preprandial, once daily before breakfast in a single dose

U/ml (range 337–3880 U/ml). The mean level of serum creatinine was 0.57 mg/dl (range 0.40–0.93 mg/dl). The mean dosage of CSA at the start of treatment was 208.3 mg/day (range 175–275 mg/day).

Pharmacokinetics of CSA in individual patients

The pharmacokinetics of CSA in individual patients is shown in Fig. 1. Mean ± standard deviation (SD) AUC_{0-6} was 4075.0 ± 1454.9 ng h/ml. Mean ± SD blood concentrations were as follows: C0, 157.3 ± 41.4 ng/ml; C2, 1222.6 ± 523.8 ng/ml; C4, 566.0 ± 202.7 ng/ml; C6, 340.7 ± 160.2 ng/ml. In all of the patients, the CSA peak concentration appeared at 2 h after administration (C2).

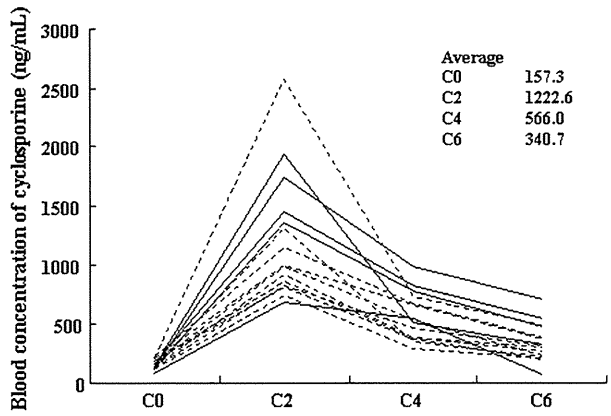

Fig. 1 Pharmacokinetics of cyclosporine in individual patients. *Solid* and *broken lines* represent patients with preprandial and postprandial administration, respectively

Correlation of AUC_{0-6} with C0, C2, C4, and C6

Correlations of AUC_{0-6} with C0, C2, C4, and C6 are shown in Fig. 2. C2, C4, and C6 correlated significantly with AUC_{0-6} ($R = 0.910$, 0.603, and 0.673; $P < 0.0001$, 0.0007, and 0.0002). The strongest positive correlation was noted between AUC_{0-6} and C2 ($R = 0.910$; $P < 0.0001$). C0 did not correlate with AUC_{0-6} ($R = 0.052$).

Comparison of CSA blood level between daily postprandial administration in a divided dose and a single dose before breakfast

CSA blood level is compared between postprandial administration in a divided dose and a single dose before breakfast in Fig. 3. The CSA C0 level was significantly lower when administered once daily before breakfast than when administered in the divided dose after meals ($P = 0.020$). There were no differences in blood levels (AUC_{0-6}, C2, and C6) between administration in the divided dose after meals and once daily.

Discussion

We investigated the pharmacokinetics of CSA in patients with progressive DM-IP. Blood CSA level peaked at C2 in all patients. AUC_{0-6}, which most markedly reflects the immunosuppressive effect, was significantly correlated with all sampling points after CSA administration, especially C2, but not C0. It has also been reported that AUC most strongly correlated with C2 while it was not correlated with C0 in the transplantation field [7] and that AUC was correlated with C2 in psoriasis and nephritic syndrome

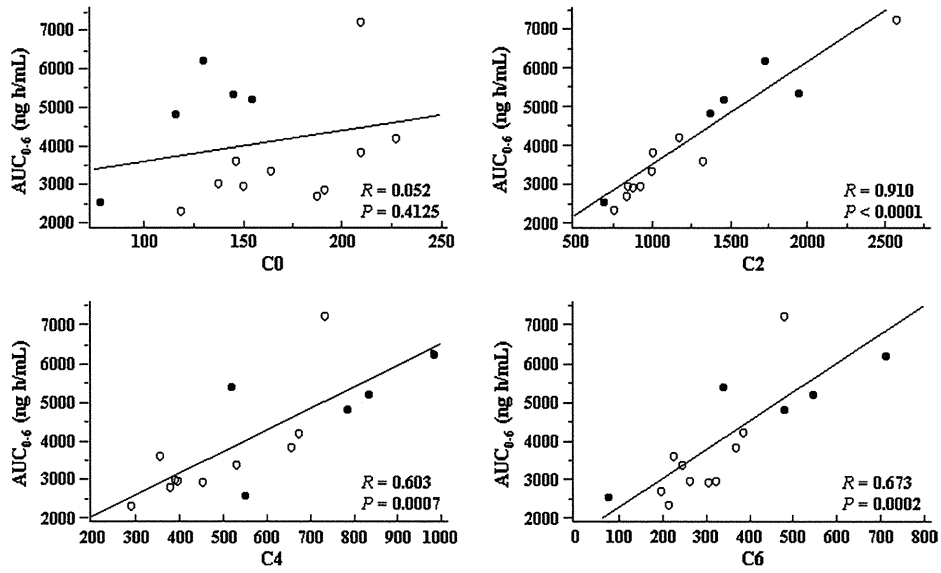

Fig. 2 Correlation of AUC_{0-6} with C0, C2, C4, and C6. *Closed* and *open circles* represent patients with preprandial and postprandial administration, respectively

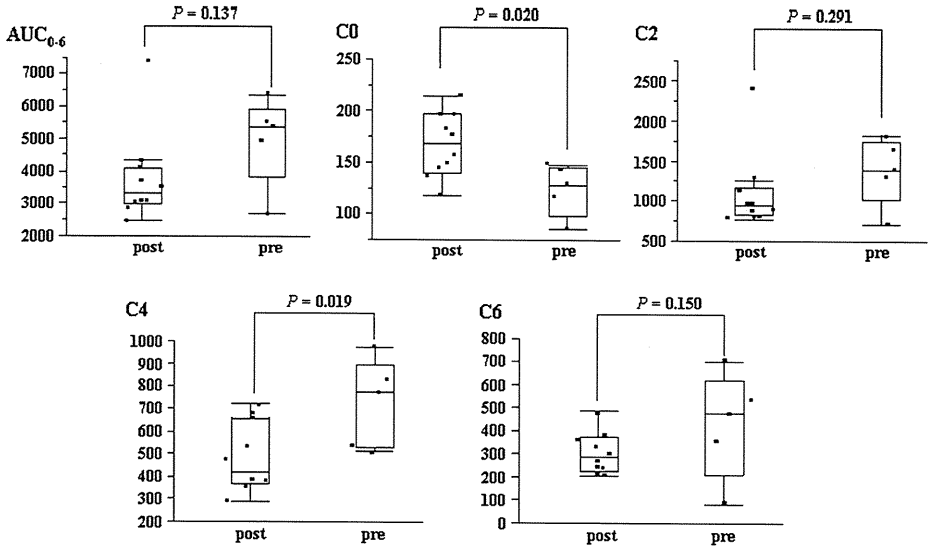

Fig. 3 Comparison of blood cyclosporine level between postprandial daily administration in two doses and preprandial, once daily administration; *Pre* preprandial, once daily before breakfast in a single dose; *Post* postprandial, twice daily in a divided dose

[9, 10]. Our study is the first report to reveal the dynamics of the blood CSA level in the field of CVD, in which the importance of C2 monitoring was clarified.

A standard regime of CSA/steroids combination therapy for progressive DM-IP has not been established. It has been reported that prognosis is favorable and respiratory function improved when CSA administration is initiated early after diagnosis of DM-IP [2, 4, 11]. The dosage of CSA for DM-IP was 100–300 mg/day in these previous reports. We previously treated 16 progressive DM-IP patients with steroids and CSA in an early stage and found that the outcome was more favorable when the dose of CSA was high [4]. Combining these findings with those of the present study, blood CSA level should be controlled based on C2, because the CSA absorption rate varies markedly among individuals.

The CSA C2 level is controlled at about 800 ng/ml in the field of transplantation [12], and an increase in the incidence of adverse effects at a CSA C0 level exceeding 200 ng/ml has been reported [13]. In this study, the mean CSA C2 and C0 levels were 1128.8 and 157.3 ng/ml, respectively. Infection could be treated by repeated surveillance and early treatment without development of drug-induced severe adverse events. Further investigation is needed to reveal the association between clinical and adverse effects and the CSA level in the blood, particularly regarding C0 and C2.

The dosing regimen of CSA may influence the blood CSA level. We compared the blood level between the postprandial divided dose and preprandial once-a-day dose groups. C2 was the peak blood level in both groups, and there were no differences in the blood levels (AUC_{0-6}, C2, and C6) between the once-a-day group and the divided dose group, while C0 was significantly lower in the once-a-day group. As recently proposed in the transplantation and the nephritic syndrome fields, preprandial, once daily administration may be more useful than postprandial administration in divided doses [14, 15]. Our data support these proposals.

CSA has recently been used for CVD-associated IP, in addition to DM-IP. Considering the marked individual variation in pharmacokinetics of CSA, measurement of its blood level, particularly C0 and C2, is necessary to evaluate clinical and adverse effects of CSA. It was also suggested that preprandial, once daily administration is more useful to achieve maximal immunosuppressive effect and avoid adverse events. However, the sample size of this study was limited, and DM patients with IP refractory to the combination of steroids and CSA have also been reported. Further studies are needed to establish a standard therapeutic strategy for DM-IP.

Conflict of interest None.

References

1. Hirakata M, Nagai S. Interstitial lung disease in polymyositis and dermatomyositis. Curr Opin Rheumatol. 2000;12:501–8.
2. Nagasaka K, Harigai M, Tateishi M, Hara M, Yoshizawa Y, Koike T, et al. Efficacy of combination treatment with cyclosporin A and corticosteroids for acute interstitial pneumonitis associated with dermatomyositis. Mod Rheumatol. 2003;13:231–8.
3. Kuroda H, Morinaga H, Satoh C, Miyake A, Sunami K. Clinical study of 10 cases of acute or subacute interstitial pneumonia associated with dermatomyositis. Mod Rheumatol. 2003;13:313–8.
4. Kotani T, Makino S, Takeuchi T, Kagitani M, Shoda T, Hata A, et al. Early intervention with corticosteroids and cyclosporin A and 2-hour postdose blood concentration monitoring improves the prognosis of acute/subacute interstitial pneumonia in dermatomyositis. J Rheumatol. 2008;35:254–9.
5. Mahalati K, Belitsky P, Sketris I, West K, Panek R. Neoral monitoring by simplified sparse sampling area under the

concentration-time curve: its relationship to acute rejection and cyclosporine nephrotoxicity early after kidney transplantation. Transplantation. 1999;68:55–62.
6. Akhlaghi F, Gonzalez L, Trull AK. Association between cyclosporine concentrations at 2 hours post-dose and clinical outcomes in de novo lung transplant recipients. J Heart Lung Transplant. 2005;24:2120–8.
7. Levy G, Thervet E, Lake J, Uchida K, Consensus on Neoral C(2): Expert Review in Transplantation (CONCERT) Group. Patient management by Neoral C(2) monitoring: an international consensus statement. Transplantation. 2002;73:S12–8.
8. Takizawa H, Shiga J, Moroi Y, Miyachi S, Nishiwaki M, Miyamoto T. Interstitial lung disease in dermatomyositis: clinicopathological study. J Rheumatol. 1987;14:102–7.
9. Umezawa Y, Ozawa A. Optimal time for therapeutic drug monitoring of cyclosporine microemulsion in patients with psoriasis. Int J Dermatol. 2007;46:763–6.
10. Naito M, Takei T, Eguchi A, Uchida K, Tsuchiya K, Nitta K. Monitoring of blood cyclosporine concentration in steroid-resistant nephrotic syndrome. Intern Med. 2008;47:1567–72.
11. Yamasaki Y, Yamada H, Yamasaki M, Ohkubo M, Azuma K, Matsuoka S, et al. Intravenous cyclophosphamide therapy for progressive interstitial pneumonia in patients with polymyositis/dermatomyositis. Rheumatology (Oxford). 2007;46:124–30.
12. Uchida K, Tominaga Y, Haba T, Katayama A, Sato T, Matsuoka S, et al. Usefulness of two-point AUC(0–4) monitoring in maintenance renal transplant patients. Transplant Proc. 2001;33:3128–30.
13. Min DI, Perry PJ, Chen HY, Hunsicker LG. Cyclosporine trough concentrations in predicting allograft rejection and renal toxicity up to 12 months after renal transplantation. Pharmacotherapy. 1998;18:282–7.
14. Bunke M, Sloan R, Brier M, Ganzel B. An improved glomerular filtration rate in cardiac transplant recipients with once-a-day cyclosporine dosing. Transplantation. 1995;59:537–40.
15. Kusaba T, Kono Y, Hatta S, Fujino T, Yasuda T, Miura H, et al. More stable and reliable pharmacokinetics with preprandial administration of cyclosporine compared with postprandial administration in patients with refractory nephrotic syndrome. Pharmacotherapy. 2005;25:52–8.

International Journal of Cardiology 147 (2011) 271–277

Contents lists available at ScienceDirect

International Journal of Cardiology

journal homepage: www.elsevier.com/locate/ijcard

Rabbit plaque models closely resembling lesions in human coronary artery disease

Taichi Okabe [a], Masaaki Hoshiga [a,*], Nobuyuki Negoro [a], Takahiro Nakakoji [a], Kumiko Arishiro [a], Tadashi Ishihara [a], Hikaru Ueno [b], Toshiaki Hanafusa [a]

[a] First Department of Internal Medicine, Osaka Medical College, Takatsuki, Osaka 569-8686, Japan
[b] Department of Biochemistry and Molecular Pathophysiology, University of Occupational and Environmental Health, School of Medicine, Kitakyusyu 807-8555, Japan

ARTICLE INFO

Article history:
Received 27 February 2009
Received in revised form 31 August 2009
Accepted 10 September 2009
Available online 6 November 2009

Keywords:
Cholesterol
Fibrous cap
Lipid core
Smooth muscle cells

ABSTRACT

Background: A suitable animal model is required to investigate plaque biology. Here, we examined 6 rabbit models of plaque generated by balloon injury and sequential combinations of normal and high-cholesterol diets.

Methods and results: Fifty-eight male Japanese White rabbits were used. Lipid-rich macrophages accumulated in the center of the intima, and smooth muscle cells were located on the luminal side of the intima (similar to stable plaques in human coronary arteries) of a model in which balloon injury was followed by a normal diet for 4 weeks and then by a high-cholesterol diet for 4 weeks. Extending the high-cholesterol diet for a further 4 weeks increased accumulation of lipid-rich macrophages, diminished the amounts of elastic fibers and smooth muscle cells in the intima and caused the expression of matrix metalloproteinase-9 and tissue factor. All of these features are characteristic of unstable plaques. Moreover, quantitative analysis revealed that matrix metalloproteinase-9 expression and elastic-fiber content inversely correlated with statistical significance ($R^2 = 0.52$, $p = 0.0003$).

Conclusion: A high-cholesterol diet for 0 to 8 weeks after a normal diet for the first 4 weeks following balloon injury induced various arterial lesions resembling the diffuse intimal thickening, as well as stable and unstable plaques that accumulate in human coronary arteries. The present models might be useful for plaque studies.

1. Introduction

Acute coronary syndrome (ACS) is primarily induced by plaque rupture followed by thrombus formation [1–3]. Thus, the mechanisms involved in plaque formation and rupture should be determined and methods of either stabilizing plaques or preventing plaque rupture should be established to improve prognosis and avoid ACS. However, the absence of suitable and practical animal models has hindered such progress.

Vulnerable plaques in human coronary arteries feature thin fibrous caps, lipid-rich necrotic cores, accumulated inflammatory cells, and a decreased amount of extracellular matrix [1–3]. Diffuse intimal thickening (DIT) composed of smooth muscle cells (SMC), type I collagen, and proteoglycans are thought to form during adolescence [4,5], and DIT might be a requirement for the later formation of a fibrous cap (inner layers of SMC overlying lipid-rich macrophages) [6,7]. The introduction of animal models exhibiting a variety of such lesions should facilitate plaque study. Apolipoprotein E-null or LDL receptor-deficient mice have been used as animal models of atherosclerogenesis. However, the mouse is not entirely appropriate for extrapolation to the human condition, since its cholesterol-transport system and the composition of its atherosclerotic lesions (e.g., macrophages with a far greater propensity to invade the media) fundamentally differ from those in humans [8,9]. Another popular animal model comprises rabbits fed with a high-fat diet. Although atheromas consisting of lipid-rich macrophages usually form in rabbits fed with >0.5% cholesterol, such atheromas lack a fibrous cap [10–13]. However, atheromas with fibrous caps can develop in rabbits fed with a lower cholesterol ratio (<0.5%) in the diet over a period of >6 months [14,15]. However, this model requires a substantial time, and thus financial investment.

Here, we analyzed data from six rabbit models that were fed with sequential combinations of normal and high-cholesterol diets following arterial balloon injury. Our models developed a variety of arterial lesions that seem to resemble some types of plaques encountered in human coronary arteries.

2. Materials and methods

2.1. Animal experimental protocols

The present investigation conformed to the *Guide for the Care and Use of Laboratory Animals* published by the US National Institutes of Health (NIH Publication No. 85-23, revised 1996). The Osaka Medical College Animal Care and Use Committee approved all of the animal experiments. Fifty-eight male Japanese White rabbits (Kitayama Labes, Nagoya, Japan) weighing 2.5 to 3.0 kg individually housed in stainless steel cages were anesthetized with sodium pentobarbital (25 mg/kg), and the right carotid arteries were injured with a balloon catheter as described previously [16]. Briefly, a 2.75 mm-PTCA balloon catheter (Boston Scientific Corp., Natick, MA, USA) was advanced into the right

* Corresponding author. First Department of Internal Medicine, Osaka Medical College, 2-7 Takatsuki, Osaka 569-8686, Japan. Tel.: +81 72 683 1221; fax: +81 72 683 1801.
E-mail address: in1026@poh.osaka-med.ac.jp (M. Hoshiga).

0167-5273/$ – see front matter © 2009 Elsevier Ireland Ltd. All rights reserved.
doi:10.1016/j.ijcard.2009.09.528

carotid artery, inflated with 6 atm and denuded three times. The rabbits were then provided with either a high-cholesterol diet containing 1.0% cholesterol and 6.0% coconut oil (Oriental Yeast Co., Tokyo, Japan) or a normal chow diet for various periods.

We established 6 rabbit models as follows (Fig. 1). Model 1 ($n=6$), balloon injury, followed by the normal diet for 4 weeks; Model 2 ($n=11$), balloon injury, followed by the normal diet for 4 weeks and then the high-cholesterol diet for a further 4 weeks; Model 3 ($n=10$): high-cholesterol diet for 4 weeks, followed by balloon injury and then the high-cholesterol diet for a further 4 weeks; Model 4 ($n=10$), balloon injury, followed by the high-cholesterol diet for 4 weeks; Model 5 ($n=11$), balloon injury, followed by the normal diet for 4 weeks and then the high-cholesterol diet for 8 weeks; Model 6 ($n=10$), balloon injury, followed by the normal diet for 8 weeks and then the high-cholesterol diet for 4 weeks. At the end of each protocol, the rabbits were sacrificed by an intravenous injection of an overdose of sodium pentobarbital. The carotid arteries were perfusion-fixed with 4% paraformaldehyde, sectioned at 5 mm, fixed again with either 4% paraformaldehyde or methanol-Carnoy's fixative, and embedded in paraffin. Some carotid arteries from each model were embedded in Tissue-Tek O.C.T. compound (Sakura Finetechnical, Tokyo, Japan) and their frozen sections were stained with Oil red O. At the time of sacrifice, thrombotic occlusion of the injured carotid artery was evident in only 2 of 58 rabbits and both were from Model 5.

2.2. Primary antibodies

The primary antibodies comprised mouse monoclonal antibodies against rabbit macrophages (RAM11; Dako); human α-smooth muscle (SM) actin (1A4; Sigma-Aldrich); human proliferative cell nuclear antigen (PCNA; Dako); human matrix metalloproteinase (MMP)-9 (56-2A4; Daiichi Fine Chemicals, Toyama, Japan); and rabbit tissue factor (American Diagnostica, Inc.).

2.3. Histopathological examination

Paraffin-embedded tissues were sectioned at 3 μm, and visualized by either hematoxylin/eosin or Elastica van Gieson staining. Some sections were immunohistochemically analyzed using labeled streptavidin–biotin, as described [17]. Antigen retrieval by heating in Target Retrieval Solution (code No. S3307, Dako Cytomation, Glostrup, Denmark) was added to the procedure to immunostain tissue factor.

2.4. Histomorphometry

Two experts (T.N. and K.A.) blinded to the experimental regimes performed the histopathological analyses. Elastica van Gieson stained sections with the greatest amount of luminal narrowing due to neointima were identified from each carotid artery segment. Planimetry was performed on digitized images at ×40 magnification (Micro Computer Imaging Device; Imaging Research Co., Canada). Absolute histomorphometric measurements included the luminal area, the area bounded by the internal elastic lamina, and the area bounded by the external elastic lamina (overall vessel size). Macrophage and vascular SMC contents in the intimal area were calculated as ratios (%) of the RAM11-positive area/intimal area and of the α-SM actin-positive area/intimal area, respectively, using the NIH ImageJ Program. The ratio of proliferating cells was calculated as the number of PCNA-positive cells/the number of whole cells. MMP-9 and tissue factor expression were calculated in immunohistochemical staining as ratios (%) of MMP-9-positive area/intimal area and of tissue factor-positive area/intimal area, respectively, using the NIH ImageJ Program. Elastic-fiber contents were calculated as ratios (%) of the area of elastic fibers (determined as black in elastic van Gieson staining/intimal area using the NIH ImageJ Program).

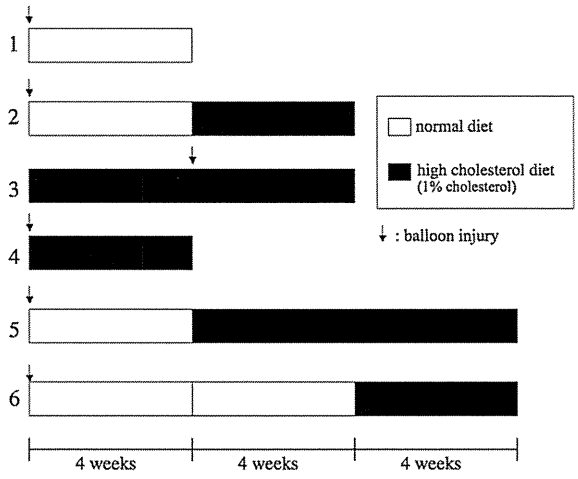

Fig. 1. Study protocols. Arrow indicates balloon injury. Unfilled and filled boxes indicate normal or high-cholesterol diets, respectively.

2.5. Serum lipid and liver enzyme levels

Blood was collected from the femoral artery under general anesthesia when the rabbits were injured and from the ear artery when they were sacrificed. Levels of total cholesterol, triglycerides, AST and ALT were measured on a Hitachi 7180 autoanalyzer using Wako reagents (Wako Pure Chemical Industries, Osaka, Japan).

2.6. Gelatin zymography

In Models 2 and 5, to detect gelatinolytic activity in the protein extract of carotid artery, zymographic analysis with a 7.5% acrylamide gel containing 0.2% gelatin was performed according to the method of Aikawa et al. [18]. Briefly, after electrophoresis under nonreducing conditions, the substrate gels were soaked twice with Triton-X-100 solution (2.5%) to remove SDS. The gels then were incubated in 50 mmol/L Tris–HCl, pH 7.4, 0.15 mol/L NaCl, 5 mmol/L CaCl2, 0.02% NaN3, and 0.05% Brij 35 for 24 h at 37 °C. The lysis of the substrates in the gels was visualized by staining with 2.5% Coomassie brilliant blue (SigmaChemical Co).

2.7. Statistical analysis

Data are expressed as means ± SEM. Data were statistically analyzed using the software package JMP7.0.1 (SAS Institute, Cary, NC, USA). An unpaired *t*-test was used to compare between 2 groups. One-way ANOVA and Tukey–Kramer multiple range test were used to compare among multiple groups. Relationships of interest were determined using Pearson's correlation analysis. A value of $p<0.05$ was considered to indicate statistical significance.

3. Results

3.1. Serum lipid and liver enzyme levels

All animals survived the study. Table 1 shows serum lipid profiles and liver enzymes in each rabbit models. After 4 weeks on the high-cholesterol diet (in Models 2, 4 and 6), serum total cholesterol increased, whereas serum triglycerides remained unchanged. After 8 weeks on the high-cholesterol diet (Models 3 and 5), serum cholesterol and triglyceride levels increased. Liver enzymes did not vary significantly but AST in Model 4 increased significantly.

3.2. Normal diet for 4 weeks after balloon injury

Neointima formed in balloon-injured carotid arteries after 4 weeks of feeding with the normal diet (Model 1) [intima/media ratio (I/M): 0.48 ± 0.04] (Fig. 2). Most cells within this neointima stained positively for α-SM actin (Fig. 3A), indicating that most of them were SMC. Almost no macrophages were stained (Fig. 3B). No intima formed in contralateral non-injured carotid artery (data not shown). Feeding with the high-cholesterol diet for the next 4 weeks (Model 2) increased the size of the intimal area but the statistical significance was not found (Fig. 2). The center of the intima (asterisks in Fig. 3D and E) contained foamy cells, of which most were macrophages containing lipids (detected by Oil red O staining in Fig. 3F), and spindle-shaped SMC were located on the luminal side. The arterial lesion in Model 2 resembled a fibrous cap overlying a lipid core.

3.3. High-cholesterol diet before and immediately after balloon injury

Fig. 3G–H shows that macrophages and SMC were diffusely located within the intima of rabbits fed with a high-cholesterol diet either before (Model 3) or immediately after balloon injury (Model 4) and a fibrous cap overlying a lipid core was not evident. Lipid-rich macrophages were located in the media of both Models 3 (open triangles in Fig. 3H and I) and 4 (data not shown). In addition to the intima, the cell-type composition of Models 3 and 4 were similar, but the areas of both intima and media were greater in Model 3 (Fig. 2).

3.4. Extending the duration of feeding with a high-cholesterol diet

After balloon injury followed by 4 weeks on the normal diet, rabbits of Models 2 and 5 were fed with a high-cholesterol diet for 4 and

Table 1
Lipid profiles and liver enzymes in each models.

Model	1	2	3	4	5	6
Total cholesterol (mmol/L)	1.02 ± 0.12	16.4 ± 2.75*	31.1 ± 2.75*,†	17.0 ± 3.03*,‡	30.5 ± 2.41*,†,‡	15.7 ± 2.32*,‡,‖
(Parenthesis in mg/dL)	(39.5 ± 4.5)	(633 ± 106)	(1200 ± 106)	(655 ± 117)	(1180 ± 93.0)	(607 ± 89.5)
Triglyceride (mmol/L)	0.25 ± 0.040	0.24 ± 0.076	1.02 ± 0.19*,†	0.16 ± 0.019*,‡	0.93 ± 0.18*,§	0.36 ± 0.077‡,‖
(Parenthesis in mg/dL)	(21.9 ± 3.5)	(21.0 ± 6.6)	(89.9 ± 16.8)	(14.1 ± 1.7)	(81.6 ± 16.1)	(31.5 ± 1.1)‡
AST (U/L)	21.2 ± 2.8	26.4 ± 6.8	48.1 ± 12.5*	28.9 ± 5.7	42.0 ± 10.6	21.6 ± 1.4‡
ALT (U/L)	40.2 ± 8.9	43.1 ± 7.2	63.1 ± 16.1	45.1 ± 5.1	53.4 ± 10.8	39.6 ± 9.9

Mean ± SEM. $p<0.05$ vs. Model 1*, Model 2†, Model 3‡, Model 4§, Model 5‖. AST: Aspartate Aminotransferase. ALT: Alanine Aminotransferase.

8 weeks, respectively. The intimal area was significantly greater in Model 5 than in Model 2 (I/M ratio, 1.25 vs. 0.73) (Fig. 2). Immunohistochemical staining of Model 5 showed far fewer SMC (Fig. 3J) and an intima full of macrophages with lipids (Fig. 3K and L). Our results indicated that longer exposure to a high-cholesterol diet led to a decrease in the amount of intimal SMC and an increase in accumulation of lipid-rich macrophages. An important finding was that the fibrous cap composed of spindle-shaped SMC (lines with arrows in Fig. 3D and J) was thinner in Model 5 than in Model 2 (the thickness of the fibrous cap: 150 ± 31 μm in Model 2 vs. 84 ± 12 μm in Model 5, $p<0.01$).

Histological analysis of arteries from rabbits, who were fed with a normal diet for 8 (Model 6) and 4 (Model 2) weeks and then a high-cholesterol diet for the next 4 weeks following balloon injury, showed significantly increased amounts of SMC and reduced accumulation of macrophages in the intima, respectively (Fig. 3M and N). However, the intimal area itself did not differ between the two models (Fig. 2).

3.5. Cell proliferation

The proliferative activity of SMC in the fibrous cap structure in the luminal side of the intima was <6% even in Model 5 (high-cholesterol diet for 8 weeks; Fig. 4E). In contrast, the proliferative activity of foam cells was much higher (25% in Model 5) (Fig. 4F).

3.6. Expression of MMP-9 and tissue factor, and elastic-fiber content

Both MMP-9 and tissue factor were readily detectable in the arterial intima of rabbits fed with a high-cholesterol diet for 4 and 8 weeks (Fig. 5A–D). More areas were positive for MMP-9 and tissue factor in Model 5 than in Model 2 (Fig. 5G and H). Almost no positive staining for MMP-9 and tissue factor was found in SMC-rich intima in Model 1 (data not shown). In addition, gelatin zymography revealed that gelatinolytic activities at 92 kDa (pro-MMP-9), 80 kDa (an activated form of MMP-9), 72 kDa (pro-MMP-2), and 68 kDa (an activated form of MMP-2) were higher in carotid arteries in Model 5 than those in Model 2 (Fig. 5I).

We also stained for elastic fibers (Elastica van Gieson staining). SMC-rich area in both intima and media in Model 1 was abundant in elastic fibers (data not shown). The quantity of elastic fibers was substantial in the intima and media of arteries from Model 2 (Fig. 5E), but very sparse in the intima of Model 5 (Fig. 5F). These results indicated that more MMP-9 and tissue factor were expressed and that the elastic-fiber content decreased when the rabbits were fed with a high-cholesterol diet for 8 weeks. Moreover, quantitative analysis revealed that MMP-9 expression and elastic-fiber content inversely correlated with statistical significance ($R^2=0.52$, $p=0.0003$).

4. Discussion

Rabbits fed with a high-cholesterol diet have previously been used as an atherosclerosis model. Typical protocols comprise a high-cholesterol (>0.5%) diet for 8 to 16 weeks. However, this protocol generates lesions with lipid-rich macrophages, but no SMC-rich fibrous caps [10–13]. Feeding with a diet containing less cholesterol (0.25–0.3% instead of 0.5–1.0%) for extended periods generates arteries containing lesions with SMC-rich fibrous caps overlying lipid cores [14,15]. However, these methods require a lengthy period, 32 (0.25% cholesterol) [14] or 26 (0.3% cholesterol) weeks [15]. The time required to form SMC-rich

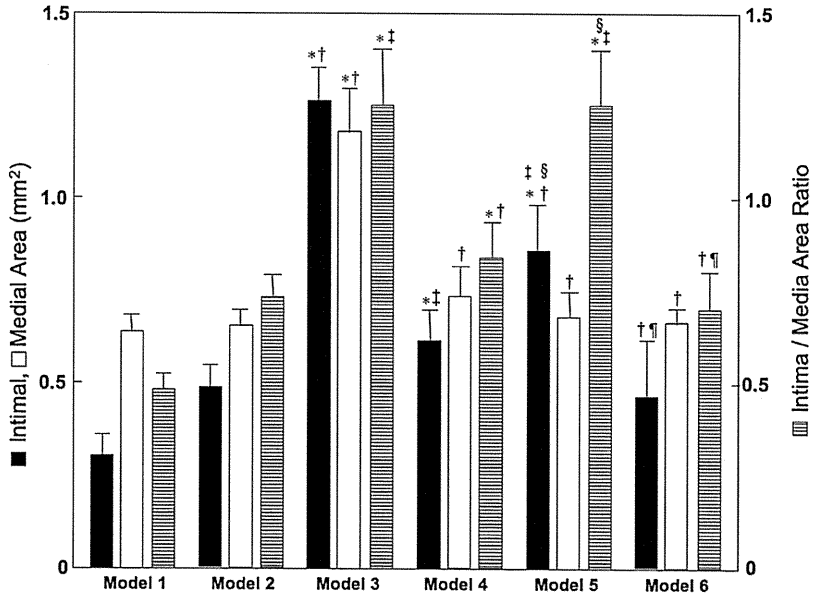

Fig. 2. Morphometric analysis of carotid lesions in each model rabbits. Comparison of intimal and medial area, and intima/media area ratio in each model rabbits. Bars represent SEM. $p<0.05$ vs. Model 1*, Model 2†, Model 3‡, Model 4§, Model 5¶.

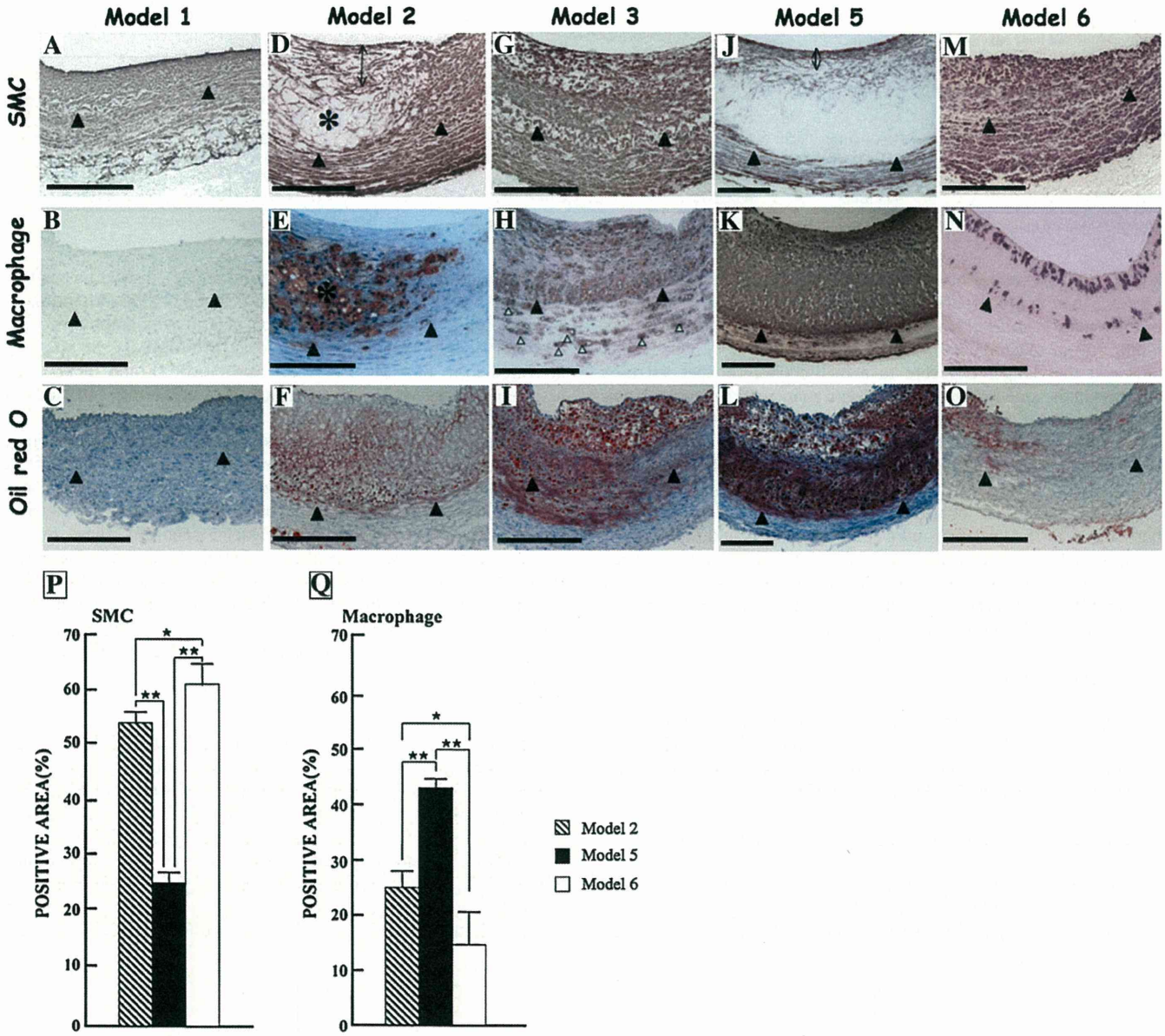

Fig. 3. Cell-type composition of experimentally induced plaques. A–O: Representative carotid artery sections from rabbits fed with various combinations of normal and high-cholesterol diets after balloon injury. A, B and C, Model 1 (normal diet 4 weeks); D, E and F, Model 2 (normal diet 4 weeks plus high-cholesterol diet 4 weeks); G, H and I, Model 3 (high-cholesterol diet 8 weeks); J, K and L, Model 5 (normal diet 4 weeks plus high-cholesterol diet 8 weeks); M, N and O, Model 6 (normal diet 8 weeks plus high-cholesterol diet 4 weeks). Immunoperoxidase staining of corresponding tissue sections stained with either anti-a smooth muscle actin (A, D, G, J, M) or anti-macrophage RAM-11 (B, E, H, K, N) monoclonal antibodies. Oil red O staining of corresponding tissue sections (C, F, I, L, O). Closed arrowhead indicates internal elastic lamina. Open arrowhead in panel H indicates macrophages in media. *Lipid core (in panels D and E). Black line with arrows, fibrous cap (in panels D and J). Scale bar, 200 mm. P and Q: Quantitative analysis of cell markers for SMC (P) and macrophage (Q) accumulation within plaque intima of Models 2 ($n=11$), 5 ($n=11$) and 6 ($n=10$). Immunoreactive areas shown as ratios (%) of entire intimal area. Bars represent SEM. *$p<0.05$; **$p<0.01$.

fibrous caps overlying lipid cores can be decreased by adding balloon injury to the high-cholesterol diet [17,18]. Based on these findings, we tested six protocols in rabbits, and histologically analyzed arteries in several ways as shown in Table 2. An important finding is that the initial feeding of a normal diet is essential for lesions to form SMC-rich fibrous caps. That is, without this initial feeding after balloon injury, macrophages widely infiltrated the intima and an SMC-rich fibrous cap-like layer did not form (Models 3 and 4). As the balloon injury produces intense inflammation, which is much different from high-fat diet, we think the timing of balloon injury and which diet is very important. One of co-authors, Ueno, showed that a lot of macrophages were shown in rabbit carotid artery at 7 days after balloon injury with normal diet [19], indicating that balloon injury produces intense inflammation. However, as shown in Fig. 3B in the present study, there was little macrophage 4 weeks after balloon injury with normal diet. Thus the initiation of high-cholesterol diet did not overlap the inflammation period by balloon injury in Models 2 and 5. In contrast, in Models 3 and 4, high-cholesterol feeding did overlap the inflammatory period by balloon injury. We think that such a difference is critical to develop atherosclerotic plaque resembling lesions in human coronary arteries. Our model required only 8 weeks to develop a fibrous cap overlying a lipid core (Model 2), which is the most efficient of the protocols reported in the literature to date.

Human coronary and carotid arteries, which are highly prone to plaque rupture, differ from other human arteries in that they easily develop intimal thickening composed of SMC from childhood, long

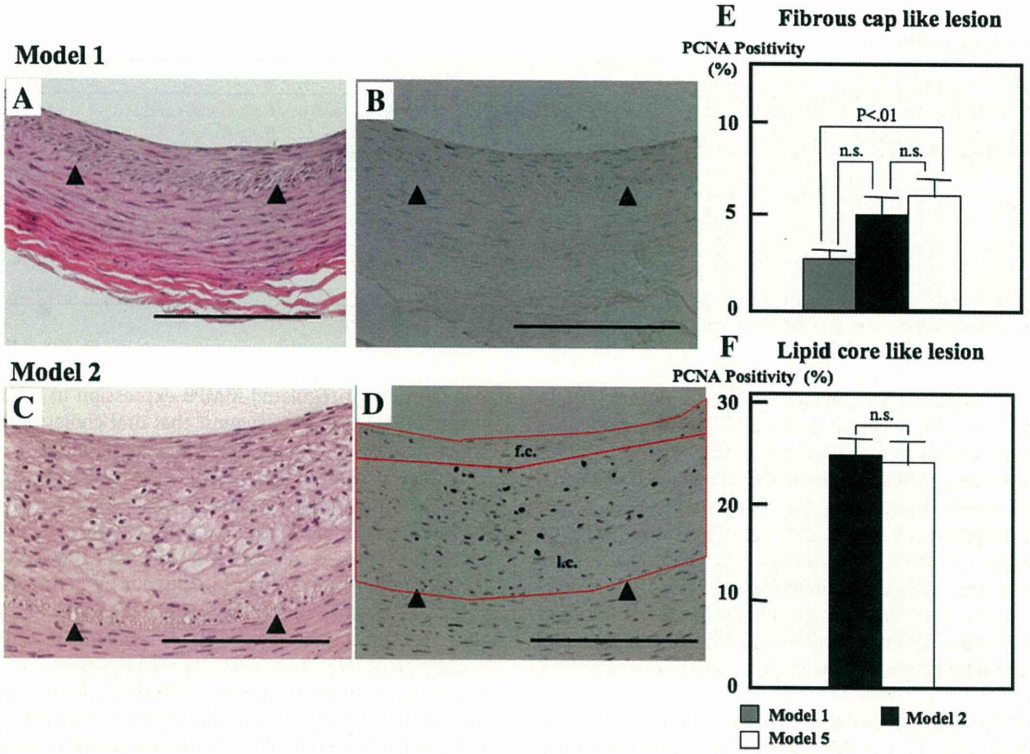

Fig. 4. Replication of vascular cells in arteries from Models 1, 2 and 5. Cell replication in Models 1 (A, B) and 2 (C, D). A, C, hematoxylin and eosin staining; B, D, immunostaining for replication marker PCNA. Arrowheads, internal elastic lamina. Scale bar, 200 μm. Quantitative immunohistochemical analyses of PCNA in fibrous cap (f.c.) region (E) and lipid core (l.c.) region (F) in Models 1, 2 and 5. Bars represent SEM.

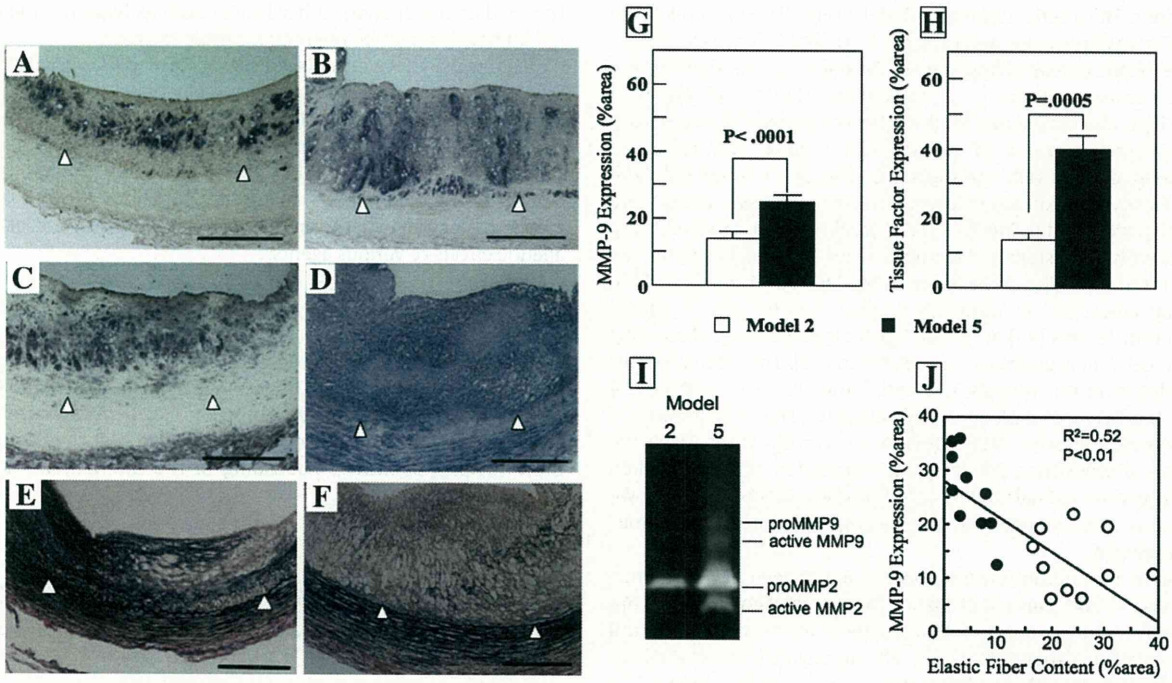

Fig. 5. Matrix metalloproteinase 9, tissue factor and elastic fibers in arteries from Models 2 and 5. Representative immunohistochemical staining with matrix metalloproteinase (MMP)-9 antibody (A and B) and tissue factor antibody (C and D), and representative Elastica van Gieson staining (E and F) in carotid artery sections from Models 2 (A, C, D) and 5 (B, D, F). White arrowhead, internal elastic lamina. Scale bar, 200 mm. Quantitative analyses of MMP-9 (G) and tissue factor (H) expression within rabbit carotid arteries from Models 2 and 5. Immunopositive areas are shown as ratios (%) of entire intimal area. Bars represent SEM. Gelatin zymogram of gelatinase activities in protein extracts of carotid arteries from Models 2 and 5 (I). Gelatinolytic activity at 92 kDa (pro-MMP-9), 80 kDa (an activated form of MMP-9), 72 kDa (pro-MMP-2), and 68 kDa (an activated form of MMP-2) was detected. Association between MMP-9-positive area (% of intima) and elastic-fiber content (% of intima) determined by immunohistochemistry and Elastica van Gieson staining (J), respectively.

Table 2
Summary of results from each models.

Model	1	2	3	4	5	6
Procedures	N.D. 4 weeks after B.I.	N.D. 4 weeks and H.C. 4 weeks after B.I.	H.C. 4 weeks before and H.C. 4 weeks after B.I.	H.C. 4 weeks after B.I.	N.D. 4 weeks and H.C. 8 weeks after B.I.	N.D. 8 weeks and H.C. 4 weeks after B.I.
Cell Composition of plaque	Only SMC	SMCs overlying macrophagess	Mixtures of SMC and macrophagess	Mixtures of SMC and macrophagess	Thin layer of SMC overlying macrophagess	Diffuse SMCs with sparse macrophagess
Presence of fibrous cap	No	Thick	No	No	Thin	Very thick
Tissue factor	No	+	n.d.	n.d.	+++	n.d.
MMP9	No	+	n.d.	n.d.	+++	n.d.
Elastic fibers	+++	+++	n.d.	n.d.	+	n.d.

N.D.: normal diet, H.C.: high cholesterol diet, B.I.: balloon injury, SMC: smooth muscle cell. n.d.: not determined.

before lipid-rich macrophages accumulate within the intima [20]. In contrast, in apoE- or LDL receptor-null mice, (a) macrophages infiltrate and lipid accumulates in the intima even at very early stages and (b) macrophages sometimes invade the media beyond the internal elastic lamina [8,9], events that are very different from those that occur during plaque development in human coronary and carotid arteries. In our plaque Models 1, 2 and 5, macrophages accumulated after SMC had accumulated in the intima, and macrophages were not readily detectable in the media. These features are similar to the pathology of human coronary arteries, although we should note the histological difference between rabbit carotid as elastic artery and human coronary as muscular artery.

Models 1, 2 and 5 among the models established in this study can be prepared sequentially (Fig. 1). The DIT lesions that develop in human coronary arteries and the neointima in our Model 1 are similar in several ways. First, both lesions were almost completely composed of SMC (Ref. 21 and Fig. 3B). Secondly, most SMC in the intima showed little proliferation either in human coronary DIT (PCNA-positive ratio is about 3% in the intima of coronary arteries from 3 months to 2 years of age [21], and less than 1% in adults [22]), which was also true for that in Model 1 (2.8% positive). Thirdly, no lipid core formed in either human or rabbit lesions. The arterial lesions in Model 2 (Fig. 3D–F) had relatively thick, SMC-rich fibrous caps overlying the foci of lipid-rich macrophages (lipid core), features resembling those of the stable plaques that develop in human coronary arteries [1–3]. In addition, the arterial lesions in Model 5 (high-cholesterol diet for 8 weeks) comprised thinned fibrous caps, decreased amounts of extracellular matrix, and increased accumulation of lipid-rich macrophages (Fig. 3J–L) compared with Model 2. Finally, the expression levels of MMP-9 and tissue factor were considerably increased in Model 5 (Fig. 5). All these characteristics are consistent with the histological features of unstable plaques in human coronary arteries [1–3] and the lesion in Model 5 corresponds to "thin fibrous cap atheroma" in Virmani's original classification of human atherosclerotic lesions [23] or "Grade 3 pathological intimal thickening with foam cells" in Nakashima's classification [24]. The arterial lesions that developed in our Models 1, 2 and 5 thus seem to respectively resemble the DIT, stable plaques, and unstable plaques that occur in human coronary arteries. Nakashima et al. recently emphasized the importance of preexisting DIT for plaque formation, which is seldom present in previous animal models including swine model [25]. Here, we established an animal model with preexisting DIT before atheromatous plaque developed.

We found a significant inverse correlation between MMP9 expression and elastic-fiber content of plaque in our rabbit models (Fig. 5J). Accumulating evidence suggests that MMP9 is one of the most critical factors involved in plaque rupture [26–28]. Among various extracellular matrix substrates for MMP9, elastin degradation, which is induced by active MMP9, correlates with plaque disruption in ApoE knockout mice [28]. We showed here that extending the duration of cholesterol feeding from 4 to 8 weeks increased MMP9 expression (and its activity) and decreased the elastic-fiber content in rabbit arteries. In addition, Aikawa et al. have reported that a normal diet followed by a cholesterol diet results in down-regulated MMP9 expression in rabbit atherosclerotic plaque [18]. These data suggest that oral cholesterol might modulate MMP9 activity and thereby plaque vulnerability.

A recent review lists seven criteria for any optimal model of atherosclerotic plaque [8]. Our Models 2 and 5 satisfied four of these as follows: the atherosclerotic processes were very similar to those involved in human coronary arteries; both the cap/core ratio and the cellular composition of the intima in our models were close to those in human atheroma; our models were reproducible and require only 12 weeks for completion, which is convenient and should facilitate investigations; the 3-hydroxy-3-methyl-glutaryl-CoA reductase inhibitor, statin, stabilized plaque in our Model 5 (manuscript in preparation), which might satisfy the criterion that the response to treatment in an ideal animal model should have the potential for duplication in humans. However, our models still lack the other three features in that review [8] as follows: the same vulnerability to rupture as its human counterpart; plaque rupture in the model should occur without the need for manipulations, and plaque rupture should be accompanied by platelet-rich fibrin thrombi. None of our models offers reproducible plaque rupture or evidence of thrombo-occlusion even when we have tried to extend the high-cholesterol diet in Model 5 for additional 4 weeks ($n=6$, data not shown). Other factors such as hypertension and local inflammation might be required for these to occur.

In conclusion, we established six rabbit models with arterial injury that were subsequently fed with combinations of normal and high-cholesterol diets. The arterial lesions in our Models 2 and 5 were easily and reproducibly induced, and relatively quickly (12 weeks) exhibited at least some of the features of stable and unstable plaques in humans. Use of our models might facilitate investigations of some aspects of plaque biology relevant to human coronary arteries, and of the therapeutic effects of various agents.

Acknowledgements

This study was supported in part by the High-Tech Research Program of Osaka Medical College, Osaka, Japan to MH and NN.

We thank Ms. E. Kohbayashi for her excellent technical support. The authors of this manuscript have certified that they comply with the Principles of Ethical Publishing in the International Journal of Cardiology [29].

References

[1] Fuster V. The pathogenesis of coronary artery disease and the acute coronary syndrome. N Engl J Med 1992;326:242–50.
[2] Falk E, Shah PK, Fuster V. Coronary plaque disruption. Circulation 1995;92:657–71.
[3] Libby P. Molecular bases of the acute coronary syndrome. Circulation 1995;91:2844–50.
[4] Stary HC, Chandler AB, Dinsmore RE, et al. A definition of advanced types of atherosclerotic lesions and a histological classification of atherosclerosis. Circulation 1995;92:1355–74.
[5] Stary HC. Evolution and progression of atherosclerotic lesions in coronary arteries of children and young adults. Arteriosclerosis 1989;9(suppl I):I–19-I-32.
[6] Schwartz SM, deBlois D, O'Brien E. The intima. Soil for atherosclerosis and restenosis. Circ Res 1995;77:445–65.

[7] Newby AC, Zaltsman AB. Fibrous cap formation or destruction—the critical importance of vascular smooth muscle cell proliferation, migration and matrix formation. Cardiovasc Res 1999;41:345–60.
[8] Cullen P, Baetta R, Bellosta S, et al. MAFAPS Consortium. Rupture of the atherosclerotic plaque: does a good animal model exist? Arterioscler Thromb Vasc Biol 2003;23: 535–42.
[9] Napoli C, Palinski W. Unraveling the mechanisms of plaque rupture in murine models. Circulation 2002;106:e186.
[10] Wissler RW, Vesselinovitch D. Experimental models of human atherosclerosis. Ann N Y Acad Sci 1968;149:907–22.
[11] Jokinen MP, Clarkson TB, Prichard RW. Animal models in atherosclerosis research. Exp Mol Pathol 1985;42:1–28.
[12] Stehbens WE. An appraisal of cholesterol feeding in experimental atherogenesis. Prog Cardiovasc Dis 1986;29:107–28.
[13] Vesselinovitch D. Animal models and the study of atherosclerosis. Arch Pathol Lab Med 1988;112:1011–7.
[14] Kockx MM, De Meyer GR, Buyssens N, Knaapen MW, Bult H, Herman AG. Cell composition, replication, and apoptosis in atherosclerotic plaques after 6 months of cholesterol withdrawal. Circ Res 1998;83:378–87.
[15] Kolodgie FD, Katocs AS, Largis EE, et al. Hypercholesterolemia in the rabbit induced by feeding graded amounts of low-level cholesterol: methodological considerations regarding individual variability in response to dietary cholesterol and development of lesion type. Arterioscler Thromb Vasc Biol 1996;16:1454–64.
[16] Negoro N, Hoshiga M, Seto M, et al. The kinase inhibitor fasudil (HA-1077) reduces intimal hyperplasia through inhibiting migration and enhancing cell loss of vascular smooth muscle cells. Biochem Biophys Res Commun 1999;262:211–5.
[17] Stadius ML, Gown AM, Kernoff R, Collins CL. Cell proliferation after balloon injury of iliac arteries in the cholesterol-fed New Zealand White rabbit. Arterioscler Thromb Vasc Biol 1994;14:727–33.
[18] Aikawa M, Rabkin E, Okada Y, et al. Lipid lowering by diet reduces matrix metalloproteinase activity and increases collagen content of rabbit atheroma: a potential mechanism of lesion stabilization. Circulation 1998;97:2433–44.
[19] Arakawa H, Qian JY, Baatar D, Karasawa K, Asada Y, Sasaguri Y, et al. Local expression of platelet-activating factor-acetylhydrolase reduces accumulation of oxidized lipoproteins and inhibits inflammation, shear stress-induced thrombosis, and neointima formation in balloon-injured carotid arteries in nonhyperlipidemic rabbits. Circulation 2005;111:3302–9.
[20] Schwartz SM. The intima. A new soil. Circ Res 1999;85:877–9.
[21] Gordon D, Reidy MA, Benditt EP, Schwartz SM. Cell proliferation in human coronary arteries. Proc Natl Acad Sci U S A 1990;87:4600–4.
[22] Ikari Y, McManus BM, Kenyon J, Schwartz SM. Neonatal intima formation in the human coronary artery. Arterioscler Thromb Vasc Biol 1999;19:2036–40.
[23] Virmani R, Kolodgie FD, Burke AP, Farb A, Schwartz SM. Lessons from sudden coronary death. A comprehensive morphological classification scheme for atherosclerotic lesions. Arteioscler Thromb Vasc Biol 2000;20:1262–75.
[24] Nakashima Y, Fujii H, Sumiyoshi S, Wight TN, Sueishi K. Early human atherosclerosis. Accumulation of lipid and proteoglycans in intimal thickenings followed by macrophage infiltration. Arteioscler Thromb Vasc Biol 2007;27:1159–65.
[25] Nakashima Y, Wight TN, Sueishi K. Early atherosclerosis in humans: role of diffuse intimal thickening and extracellular matrix proteoglycans. Cardiovasc Res 2008;79: 14–23.
[26] Brown DL, Hibbs MS, Kearney M, Loushin C, Isner JM. Identification of 92-kD gelatinase in human coronary atherosclerotic lesions. Association of active enzyme synthesis with unstable angina. Circulation 1995;91:2125–31.
[27] Blankenberg S, Luc G, Ducimetière P, et al. Interleukin-18 and the risk of coronary heart disease in European men: the Prospective Epidemiological Study of Myocardial Infarction (PRIME). Circulation 2003;108:2453–9.
[28] Gough PJ, Gomez IG, Wille PT, Raines EW. Macrophage expression of active MMP-9 induces acute plaque disruption in apoE-deficient mice. J Clin Invest 2006;116: 59–69.
[29] Coats AJ. Ethical authorship and publishing. Int J Cardiol 2009;131:149–50.

Nakajima *et al. BMC Neurology* 2010, **10**:45
http://www.biomedcentral.com/1471-2377/10/45

BMC Neurology

RESEARCH ARTICLE Open Access

Visual field defects of optic neuritis in neuromyelitis optica compared with multiple sclerosis

Hideto Nakajima*†[1,2], Takafumi Hosokawa†[1], Masakazu Sugino[1], Fumiharu Kimura[1], Jun Sugasawa[3], Toshiaki Hanafusa[1] and Toshiyuki Takahashi[4]

Abstract

Background: Neuromyelitis optica (NMO) is an inflammatory demyelinating disease that predominantly affects the optic nerves and the spinal cord, and is possibly mediated by an immune mechanism distinct from that of multiple sclerosis (MS). Central scotoma is recognized as a characteristic visual field defect pattern of optic neuritis (ON), however, the differing pathogenic mechanisms of NMO and MS may result in different patterns of visual field defects for ON.

Methods: Medical records of 15 patients with NMO and 20 patients with MS having ON were retrospectively analyzed. A thorough systemic and neurological examination was performed for evaluating ON. The total number of relapses of ON and visual fields was investigated. Visual fields were obtained by Goldmann perimeter with each ON relapse.

Results: All MS patients experienced central scotoma, with 90% of them showing central scotoma with every ON relapse. However, 53% of NMO patients showed central scotoma with every ON relapse ($p = 0.022$), and the remaining 47% of patients experienced non-central scotoma (altitudinal, quadrant, three quadrant, hemianopia, and bitemporal hemianopia). Thirteen percent of NMO patients did not experience central scotoma during their disease course. Altitudinal hemianopia was the most frequent non-central scotoma pattern in NMO.

Conclusions: NMO patients showed higher incidence of non-central scotoma than MS, and altitudinal hemianopia may be characteristic of ON occurring in NMO. As altitudinal hemianopia is highly characteristic of ischemic optic neuropathy, we suggest that an ischemic mechanism mediated by anti-aquaporin-4 antibody may play a role in ON in NMO patients.

Background

Neuromyelitis optica (NMO; Devic's disease) is an idiopathic inflammatory disease of the central nervous system (CNS) that mainly affects the optic nerve and spinal cord. Traditionally, NMO is believed to differ from multiple sclerosis (MS) by causing very severe, often bilateral, optic neuritis (ON) and longitudinally extensive MRI spinal cord lesions but no MRI brain lesions or aggressive progression to disability and death [1]. Recent studies have reported a high frequency of brain MRI abnormalities in NMO patients. However, most were nonspecific and were not considered typical of MS, and hypothalamic involvement has been emphasized [2]. NMO has a more negative outcome than MS, with frequent and early relapses. Within 5 years of onset, 50% of patients have become blind in both eyes and cannot walk unassisted, and 20% die of respiratory failure due to cervical myelitis [3]. Although no controlled therapeutic trials have been specifically performed in NMO, case series and observational studies suggest that azathioprine in combination with oral steroid reduces the frequency of attacks [4,5], and rituximab and plasmapheresis can induce clinical remission of NMO [6-8]. Immuno-suppression rather than interferon β is the preferred treatment. Thus, distinguishing NMO from MS is very important for the therapeutic strategy of these disorders. Recently, clinical,

* Correspondence: in1045@poh.osaka-med.ac.jp
[1] Department of Internal Medicine I, Osaka Medical College, Takatsuki, Osaka, Japan
† Contributed equally
Full list of author information is available at the end of the article

neuroimaging, laboratory, and pathological features have been established showing that NMO is distinct from MS. Histopathological and serological findings strongly suggest the involvement of the humoral immune system [9]. In particular, detection of serum anti-aquaporin-4 (AQP4) antibody can be used to distinguish NMO from MS [10,11]

ON is the most common and often initial symptom in both NMO and MS. In acute ON, the cardinal field defect is a widespread depression of sensitivity, and visual field testing typically reveals a central scotoma, although other visual field changes such as color blindness, bitemporal hemianopia, paracentral scotoma, and altitudinal deficits have also been reported. ON in NMO tends to be more severe and recovery is less complete compared with attacks of ON in the context of MS [3]. Clinical features such as ocular pain, visual field deficits, and positive phenomena, i.e. movement-induced phosphenes, have been thought not to differ from those found in MS-associated attacks [3]. Unlike patients with MS, those with NMO experience more severe disease symptoms due to myelitis characterized by centrally located spinal cord lesions that are longer than three vertebral segments and frequent early attacks. In NMO, the pathophysiology of spinal cord lesions and relation with seropositivity for anti-AQP4 antibody are well investigated [12,13]. However, the difference of clinical symptoms or pathophysiologic findings for ON between NMO and MS have rarely been evaluated. We hypothesized that the differing pathogenic mechanisms of NMO and MS may result in different patterns of visual field defects as findings of ON. In this study, we evaluated the features of visual field defects in patients with NMO.

Method

We retrospectively analyzed the medical records of 15 patients with NMO (all women, mean age of onset: 36 ± 11, mean ± SD) and 20 patients with MS (5 men and 15 women, 29 ± 9), all of whom had ON. NMO patients fulfilled Wingerchuk's revised diagnostic criteria [14], except for NMO-IgG seropositive status. MS patients included in this study had definitive MS according to McDonald's criteria [15]. A thorough systemic and neurological examination was performed to evaluate ON. Visual field tests were performed on the Goldmann perimeter whenever visual acuity permitted. MRI was performed where deemed necessary and for those who could afford the investigation. This study received institutional review board approval and informed consent was obtained according to the Declaration of Helsinki.

Serum samples were stored at - 80°C until testing for anti-AQP4 antibody. Anti-AQP4 antibody was assessed as described previously [12,16]. Briefly, human embryonic kidney cells (HEK-293) were stably transfected with either a vector containing AQP4-cDNA or empty vector, and specimens were tested by indirect immunofluorescence using these two cell lines (with or without AQP4). Specimens were incubated with the cells for 1 h, washed in phosphate-buffered saline (PBS), incubated with Alexa Fluor 488 goat anti-human IgG (Invitrogen, Eugene, Oregon, USA) for 30 min, and washed in PBS. The cells were then fixed in 4% paraformaldehyde and mounted in Permafluor aqueous mounting media (Beckman Coulter, Marseille, France).

Statistics

All data in this study are presented as mean ± SD. Categorical variables were compared using the Mann-Whitney's U test and the Fisher's exact probability test. Significance levels were set at $P < 0.05$.

Results

A total of 35 patients were included in this study: 15 NMO and 20 MS (Table 1). There were no differences between the 2 groups in gender and disease duration. Patients with NMO were older at disease onset, exhibited an increased number of total and ON relapses, and had a higher expanded disability status scale (EDSS) score.

When comparing visual field defect patterns of ON between the 2 groups, central scotoma was present in 31 out of 33 ON episodes in MS (94%) and 39 out of 51 episodes in NMO (76%) (p = 0.041, Table 2). In 51 episodes of ON, NMO patients exhibited 12 episodes of non-central scotoma (24%). Of the visual field defect patterns other than central scotoma, NMO patients showed 5 for altitudinal, 3 for quadrant, 2 for three quadrant, 1 for hemianopia, and 1 for bitemporal hemianopia. MS patients showed 1 each for three quadrant and hemianopia (Table 2).

During the course of the disease, 90% of MS patients (18/20) showed central scotoma with every episode; however, central scotoma with every episode was present in 54% of NMO patients (8/15) (p = 0.022, Figure 1). In the remaining 7 NMO patients, 5 showed both central and non-central scotoma, and 2 patients showed non-central scotoma with every episode. In 7 NMO patients showing non-central scotoma, altitudinal hemianopia was most frequent (5/7), and the location of the altitudinal hemianopia was inferior in 3 of 5 relapses and superior in 2 relapses. Notably, all altitudinal hemianopia occurred at the initial attack of each eye (Table 3).

Discussion

A variety of visual field defects may be seen in optic neuropathies, including central, centrocecal, arcuate, altitudinal, and nasal step field defects. Central scotoma is